Cell

A Synthetic Genetic Edge Detection Program

Jeffrey J. Tabor,[1] Howard M. Salis,[1] Zachary Booth Simpson,[2,3] Aaron A. Chevalier,[2,3] Anselm Levskaya,[1] Edward M. Marcotte,[2,3,4] Christopher A. Voigt,[1,*] and Andrew D. Ellington[2,3,4]
[1]Department of Pharmaceutical Chemistry, School of Pharmacy, University of California San Francisco, San Francisco, CA 94158, USA
[2]Center for Systems and Synthetic Biology
[3]Institute for Cellular and Molecular Biology
[4]Department of Chemistry and Biochemistry
University of Texas, Austin, TX 78712, USA
*Correspondence: cavoigt@picasso.ucsf.edu
DOI 10.1016/j.cell.2009.04.048

SUMMARY

Edge detection is a signal processing algorithm common in artificial intelligence and image recognition programs. We have constructed a genetically encoded edge detection algorithm that programs an isogenic community of *E. coli* to sense an image of light, communicate to identify the light-dark edges, and visually present the result of the computation. The algorithm is implemented using multiple genetic circuits. An engineered light sensor enables cells to distinguish between light and dark regions. In the dark, cells produce a diffusible chemical signal that diffuses into light regions. Genetic logic gates are used so that only cells that sense light and the diffusible signal produce a positive output. A mathematical model constructed from first principles and parameterized with experimental measurements of the component circuits predicts the performance of the complete program. Quantitatively accurate models will facilitate the engineering of more complex biological behaviors and inform bottom-up studies of natural genetic regulatory networks.

INTRODUCTION

Living cells can be programmed with genetic parts, such as promoters, transcription factors and metabolic genes (Andrianantoandro et al., 2006; Benner and Sismour, 2005; Canton et al., 2008; Endy, 2005; Haseltine and Arnold, 2007). These parts can be combined to construct genetic versions of electronic circuits, including switches (Atkinson et al., 2003; Gardner et al., 2000; Kramer and Fussenegger, 2005; Kramer et al., 2004), logic (Anderson et al., 2007; Guet et al., 2002; Rackham and Chin, 2005), memory (Ajo-Franklin et al., 2007; Gardner et al., 2000; Ham et al., 2006), pulse generators (Basu et al., 2004), and oscillators (Atkinson et al., 2003; Elowitz and Leibler, 2000; Fung et al., 2005; Stricker et al., 2008; Tigges et al., 2009). The current challenge is to assemble multiple genetic circuits into larger programs for the engineering of more sophisticated behaviors (Purnick and Weiss, 2009).

The characterization of transfer functions or the quantitative relationship between circuit input(s) and output(s) (Bintu et al., 2005a; Tabor et al., 2009; Voigt, 2006; Weiss et al., 1999) will aid the development of accurate mathematical models (Ajo-Franklin et al., 2007; Guido et al., 2006) which will allow complex genetic programs to be examined in silico prior to physical construction. Predictive models for the design of genetic programs will drive applications in biotechnology and aid bottom-up studies of natural regulatory systems.

Edge detection is a well-studied computational problem used to determine the boundaries of objects within an image (Suel et al., 2000). This process reduces the information content in a complex image and is used in applications ranging from retinal preprocessing (Maturana and Frenk, 1963) to the analysis of microarray data (Kim et al., 2001). For a digital black and white image, a typical algorithm operates by scanning for a white pixel and then comparing the intensity of that pixel to its eight neighboring pixels. If any of the neighbors is black, the algorithm classifies those pixels as being part of an edge. The serial nature of this search process results in a computation time that increases linearly with the number of pixels in the image. We aimed to implement a parallel edge detection algorithm wherein each bacterium within a spatially distributed population functions as an independent signal processor. In this design, each bacterium (up to 10^9 individuals for a 90 mm Petri dish image) processes a small amount of local information simultaneously, and the population cooperates to find the edges.

RESULTS

A Genetic Program for Edge Detection

The genetic edge detection algorithm programs a lawn of bacteria to identify the light-dark boundaries within a projected image of light (Figures 1A and 1B). To accomplish this, each bacterium in the population executes the following pseudocode (Figure 1C): IF NOT light, produce signal. IF signal AND NOT (NOT light), produce pigment.

The "produce signal" and "produce pigment" functions make the cell generate a diffusible communication signal and a black pigment, respectively. The conversion of this pseudocode into a molecular genetic system is shown in Figure 1D.

When cells sense that they are in the dark, they produce the diffusible signal (Figure 1B). Cells that sense light do not make the signal, but are allowed to respond to it. Thus only those cells that are in the light but proximal to dark areas activate the output which results in the enzymatic production of a black pigment. The biological edge detection algorithm requires: (1) a dark

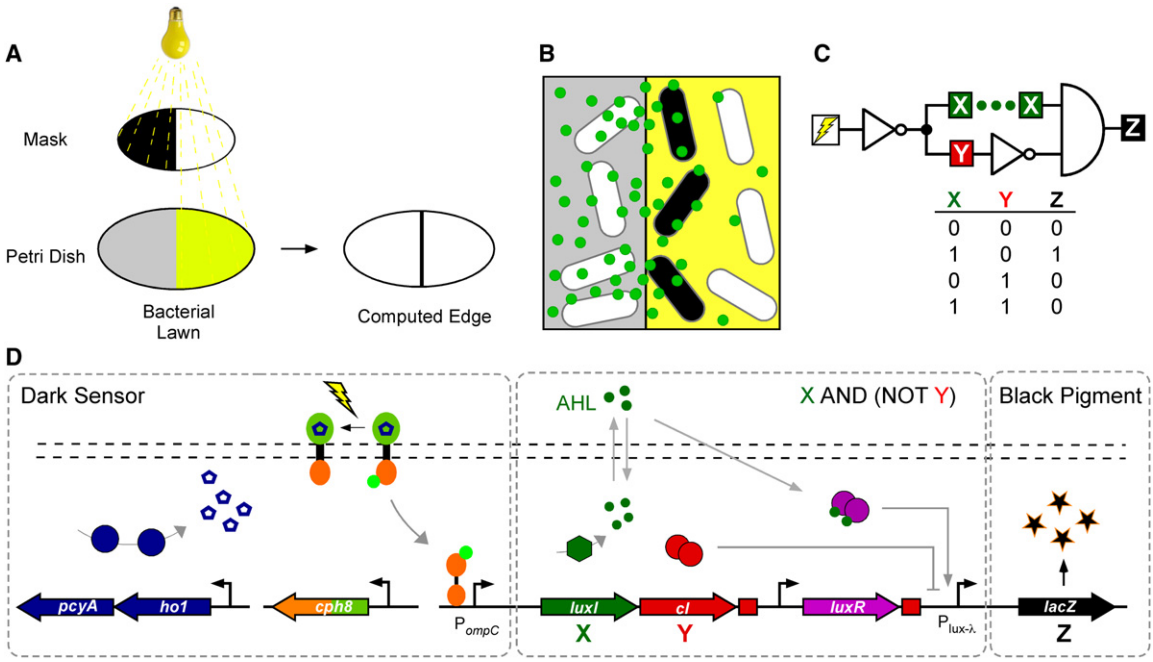

Figure 1. Bacterial Edge Detection

(A) Light is projected through a mask onto a large community (lawn) of bacteria grown on a Petri dish. The lawn computes the edges, or boundaries between light and dark regions, and visually presents the output.

(B) To find the edges, bacteria in the dark produce a communication signal (green circles) that diffuses across the dark/light boundary. Bacteria in the dark cannot respond to the communication signal. Only bacteria that are exposed to light and receive the signal become positive for the expression of a visible reporter gene. The sum of this activity over the entire two-dimensional population is equivalent to the edges of the input image.

(C) (Top) A NOT light gate (lightning box + adjacent triangle) drives a cell-cell communication circuit (green X) and an inverter (red Y + adjacent triangle). These two signals combine as inputs for a downstream AND gate (semi-circle) which drives the final output (Z). Because signal is inverted at Y, the gate driving Z can also be described as an X AND (NOT Y) gate, and it is referred to as such throughout this work. (Bottom) Z is produced in only one of four possible combinations of X and Y (presence of X, absence of Y).

(D) Conversion of the edge detection algorithm into a molecular genetic system. (Left) The light-sensitive protein Cph8 is a chimeric sensor kinase bearing the photoreceptor domain of the *Synechocystis* phytochrome Cph1 and the kinase domain of *E.coli* EnvZ (Levskaya et al., 2005). Cph8 requires the covalently associated chromophore phycocyanobilin (PCB, blue pentagons) which is produced from heme by the products of the two constitutively expressed genes *ho1* and *pcyA* (Gambetta and Lagarias, 2001). In the presence of red light, the kinase activity of Cph8 is inhibited, precluding the transfer of a phosphoryl group (light green circle) to the response regulator OmpR (orange dumbbell) and subsequent transcription from the *ompC* promoter (P_{ompC}). The dark sensor therefore functions as a NOT light transcriptional logic gate. (Center) *luxI* and *cI* are expressed polycistronically from the NOT light gate. LuxI is a biosynthetic enzyme from *V.fischeri* that produces the cell-cell communication signal 3-oxohexanoyl-homoserine lactone (AHL). CI is the transcriptional repressor protein from phage λ. AHL binds to the constitutively expressed transcription factor LuxR to activate expression from the $P_{lux-\lambda}$ promoter while CI dominantly represses it. $P_{lux-\lambda}$ therefore functions as an X AND (NOT Y) transcriptional logic gate. (Right) The output of $P_{lux-\lambda}$ is *lacZ*, the product of which (β-galactosidase) cleaves a substrate in the media to produce black pigment (Experimental Procedures). The edge detection algorithm is encoded as 10,020 basepairs of DNA, carried on three plasmid backbones (Experimental Procedures).

sensor (NOT light), (2) cell-cell communication, and (3) X AND (NOT Y) genetic logic. Each of these components is constructed as an independent genetic circuit and the behavior is characterized. This data is used to parameterize a mathematical model which in turn is used to analyze the complete system.

Construction and Characterization of Genetic Circuits

In an effort to make photographic bacteria, we previously constructed a dark sensor (Levskaya et al., 2005) based on genetic parts from the blue-green algae *Synechocystis* (Yeh et al., 1997). The sensor consists of a chimeric two-component system and a two gene metabolic pathway to make the chromophore phycocyanobilin (PCB) (Gambetta and Lagarias, 2001). To rewire the two-component system, the osmosensing domain of the *E. coli* protein EnvZ was replaced with the photoreceptor domain of the *Synechocystis* phytochrome Cph1. This programmed phosphotransfer from EnvZ to OmpR and subsequent transcription from the P_{ompC} to be repressed as a function of red light. The sensor therefore functions as a genetic circuit with NOT light logical behavior. When the dark sensor is connected to the production of β-galactosidase, a plate of bacteria can print an image of light as a pattern of black pigment (Figure 3A).

The transfer function, which characterizes how the output of a circuit varies with input at steady-state, has been shown to be a useful tool for connecting genetic circuits (Anderson et al., 2007; Bintu et al., 2005a; Voigt, 2006; Weiss et al., 1999; Yokobayashi et al., 2002). Here, the transfer function of the dark sensor is determined in response to light in the 650 nm band (Figure 2A). The dark sensor generates maximal transcriptional output at light intensities between 0.000 and 0.002W/m^2, reaches minimal

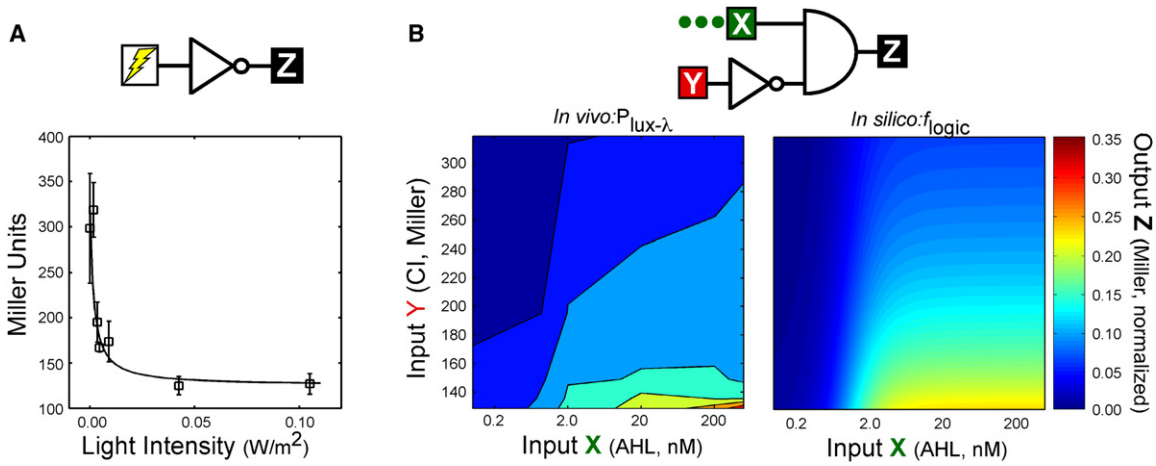

Figure 2. Transfer Functions of the Dark Sensor and X AND (NOT Y) Logic Gate

(A) The transfer function of the dark sensor is determined in batch culture (Experimental Procedures and Figure S4) and fit to a sigmoidal function (Equation 1). The error bars indicate ±1 standard deviation. (B) (Left) The transfer function of the X AND (NOT Y) logic gate as determined in batch culture experiments. AHL (X) was added exogenously to the growth media while CI (Y) levels were controlled by varying the intensity of light (Experimental Procedures and Figure S5). The data shown are single replicates of 5 assays taken over 5 separate days where the concentration of CI was altered in each assay. (Right) Mathematical Model. The output of f_{logic} (Equation 2) as a function of AHL and CI. β-galactosidase output levels (Z) for the experiment and the model are normalized by dividing by the output value in the absence of CI with maximum exogenous AHL (Experimental Procedures).

output at ~0.04W/m^2 and is repressed rapidly and continuously as a function of light (Figure 2A). The transfer function has the form

$$f_{light} = \frac{K}{K+L}(\beta_{max} - \beta_{min}) + \beta_{min} \quad (1)$$

where β_{max} = 298 and β_{min} = 125 are the maximum and minimum output values (in Miller units), L is the intensity of light (W/m^2) and the fit parameter is K = 0.0017 W/m^2 (R^2 = 0.75) (Experimental Procedures).

The edge detection algorithm also requires that neighboring bacteria communicate. It has previously been shown that *E.coli* can be programmed to communicate using the quorum sensing system from *V. fischeri* (Anderson et al., 2006; Balagadde et al., 2008; Basu et al., 2005; Weiss and Knight, 2001; You et al., 2004). We placed this communication system under the control of the dark sensor (Figure 3B). In this circuit, dark activates transcription of *luxI*, the product of which catalyzes the formation of the membrane diffusible compound 3-oxohexanoyl-homoserine lactone (AHL) (Engebrecht and Silverman, 1984). AHL binds to the constitutively expressed transcription factor LuxR to activate expression of β-galactosidase. This produces a pattern of β-galactosidase expression similar to the photographic bacteria, but with an additional blurring component due to AHL diffusion across the dark/light boundary (Figure 3B).

In addition to communication, the edge detection algorithm requires that β-galactosidase be expressed only where AHL AND light, or equivalently NOT (NOT light), are present. This requires genetic circuits that encode the NOT and AND logic functions to be combined with the NOT light circuit. Genetic logic can be constructed by rewiring regulatory interactions (Anderson et al., 2007; Cox et al., 2007; Guet et al., 2002; Mayo et al., 2006; Weiss et al., 1999). The NOT function can be achieved using a genetic inverter, which has previously been shown to invert the activity of an input promoter (Yokobayashi et al., 2002). We constructed an inverter using the *cI* gene from phage λ, the product of which forms a dimeric transcriptional repressor that turns OFF the output promoter when the input promoter is ON. By inserting the inverter between the dark sensor input and β-galactosidase output, a negative bacterial photograph can be generated where black pigment is produced only in the light (Figure 3C).

The full logic function AHL AND NOT (NOT light) is implemented at the two-input promoter $P_{lux-\lambda}$, which is activated by AHL-bound LuxR but dominantly repressed by CI. By adding a constitutively expressed copy of the *luxR* gene to the inverter, the two-dimensional transfer function of this promoter can be determined in batch culture experiments by exogenously varying AHL and light while measuring β-galactosidase activity as the output. Transcription from $P_{lux-\lambda}$ increases proportional to the concentration of AHL between 2 nM and 200 nM. At a given AHL concentration, transcription is repressed approximately 4-fold by maximal (dark) CI levels as compared to those in saturating light (Figure 2B, left). The experimental data is used to fit a two-dimensional transfer function (Figure 2B, right) that uses the Shea-Ackers formalism (Shea and Ackers, 1985) to model transcription factor binding to $P_{lux-\lambda}$ as a function of AHL (u_1) and CI (u_2) concentrations,

$$f_{logic}(u_1, u_2) = \frac{(c_0 + c_1 f_{Lux})}{1 + c_0 + c_1 f_{Lux} + c_2 f_{CI}^n + c_1 c_2 f_{Lux} f_{CI}^n} \quad (2)$$

where f_{Lux} is the concentration of LuxR dimers bound to AHL (Urbanowski et al., 2004) and f_{CI} is the concentration of dimeric CI (Koblan and Ackers, 1991). The parameters c_0 to c_2 are determined by fitting the output of f_{logic} to the transcription measurements (c_0 = 0.04, c_1 = 0.05, c_2 = 0.011, R^2 = 0.81) (Experimental Procedures) and n is 1.5. Taken together, the data in Figure 2 demonstrate that the dark sensor and the X AND (NOT Y) logic circuit function as needed for use in the edge detection algorithm. Moreover the transfer functions of the two circuits are

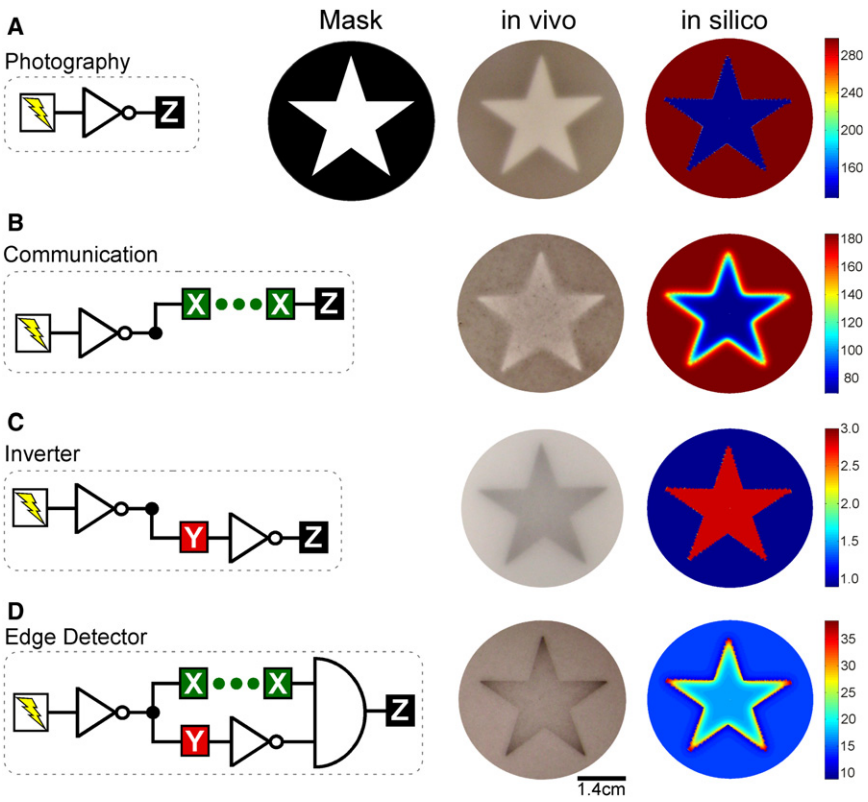

Figure 3. Construction of the Edge Detector from Individual Genetic Circuits

Various circuits are constructed and the effect on image processing is assayed (left) and compared to the mathematical model (right). The details of the genetic circuits and simulations are presented in the Experimental Procedures and Figure S2.

(A) The bacterial photography circuit, where the β-galactosidase output is expressed directly under the control of the light-sensitive $P_{ompC1157}$ promoter. This produces a positive print of the projected image.

(B) Cell-cell communication components are added by placing *luxI* under the control of the dark sensor and expressing *luxR* constitutively. This produces a positive image with an additional blurring component due to AHL diffusion.

(C) A genetic inverter is inserted between the dark sensor input and the β-galactosidase output. This produces an inverted (negative) print of the image, where the light regions are printed as dark and vice-versa.

(D) A population of cells programmed with the complete edge detector system produces black pigment only at the boundary between light and dark regions. The model solutions are reported in Miller units (color bars, right).

properly matched; transcription from the X AND (NOT Y) gate can be controlled by AHL and CI over the output ranges generated by the dark sensor.

Assembling Circuits into the Full Program

Figure 3 shows the stepwise assembly of the edge detection algorithm from the component genetic circuits. When a lawn of bacteria programmed with the edge detection algorithm is exposed to an image of light, the community prints the dark-light edges (Figure 3D), with an average edge width of 6.0 ± 1.8 mm (n = 3) (Figure 5A). Figure 4 demonstrates that the bacterial lawns can accurately solve the edges of a circle, a square, and the silhouette of a man.

Reaction-Diffusion Model

A model of the complete edge detector system is constructed based on the individually measured dark sensor and logic transfer functions f_{light} and f_{logic} (Experimental Procedures). The model quantifies the dynamics of light-dependent production of AHL and CI, AHL diffusion, production of the β-galactosidase reporter and degradation of all products. Assuming that AHL diffusion is the slowest process, the system is described by the equations,

$$\frac{\partial u_1}{\partial t} = D\nabla^2 u_1 + \kappa_1 f_{light} - \kappa_2 u_1 \quad (3)$$

$$u_2 = \kappa_3 f_{light} \quad (4)$$

$$u_3 = \kappa_4 f_{logic}(u_1, u_2) \quad (5)$$

where u_1 is the AHL concentration on the plate (nM), u_2 is the concentration of CI dimers (nM), and u_3 is the concentration of β-galactosidase in Miller Units. The diffusivity and half-life of AHL are obtained from previously published values (D = 1.67x10^{-7} cm^2/sec, κ_2 = 0.012 hr^{-1}) (Basu et al., 2005; Flagan et al., 2003). The production rate of AHL is a function of the density of the bacteria on the plate and is obtained by fitting to the edge profile (κ_1 = 0.03 nM/hr). The maximum CI and β-galactosidase concentrations are determined by fitting the experimental data to the individual transfer functions (κ_3 = 0.8 nM/Miller, κ_4 = 289 Miller) (Experimental Procedures). Because the system is an agarose plate, the reaction-diffusion model is defined on polar coordinates with a no-flux boundary condition on the outer border.

The model accurately describes the pattern of β-galactosidase on a plate of bacteria expressing the edge detector and each of the sub-circuits for each of the light patterns shown in Figures 3 and 4. The quantitative accuracy of the model is evaluated in Figure 5. Figure 5A shows a one-dimensional analysis of the circle pattern where the in silico and in vivo edge intensity profiles are compared as a function of radial distance from the center. For complex images, the edge intensity is greater at acute angles and along convex arcs than flat edges. In these areas there are more cells producing AHL per unit area. This increases the local AHL concentration and consequently the β-galactosidase output in adjacent illuminated areas. The relationship between edge intensity and the angle of line intersection is also accurately captured by the model (Figure 5B).

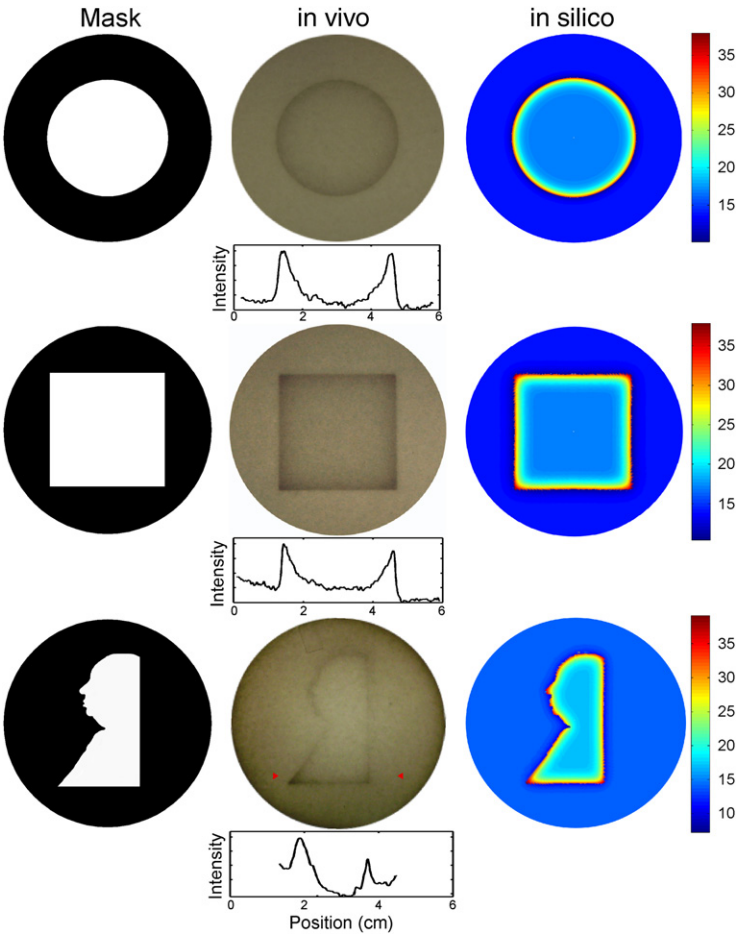

Figure 4. Edge Detection of Complex Patterns

Circle (top), square (middle) and silhouette (bottom) images are projected onto lawns of bacteria programmed with the edge detector. Signal intensities and distances are shown under each bacterial lawn. For the asymmetrical silhouette pattern, the signal intensity profile is computed for a small horizontal rectangle centered at the two red arrows. The model solutions are reported in Miller units (color bars, right).

DISCUSSION

Individual genetic circuits that mimic basic electronic functions have previously been constructed (Anderson et al., 2007; Atkinson et al., 2003; Basu et al., 2004; Elowitz and Leibler, 2000; Gardner et al., 2000; Guet et al., 2002; Ham et al., 2006; Yokobayashi et al., 2002). The next step is to understand how to combine these functions to create more complex genetic programs (Purnick and Weiss, 2009). This requires well-characterized parts and circuits that perform reliably when linked to others, without unforeseen higher-order effects (Kim and Tidor, 2003). Here, we have demonstrated that a number of well-characterized genetic circuits can be reliably combined to create a larger program. Different circuit combinations produce expected behaviors that can be predicted by a mathematical model parameterized with data from the characterization of the individual circuits. This will not be true for all circuit combinations, and understanding the origins of higher-order effects and how they can be accounted for in the design process is an outstanding challenge (Arkin and Fletcher, 2006). As the programs become larger, it will also become increasingly important to include information on how the engineered circuits impose burdens upon the host cells, including transcriptional, translational, metabolic, and energy resources (Canton et al., 2008; Tabor et al., 2008). Detailed studies of the interactions between synthetic circuits and host systems (Guido et al., 2007) may lead to new conclusions regarding regulatory and metabolic cross-talk and the ability of cells to tolerate or adapt to increased genetic load.

Logic and cell-cell communication form the core of regulatory networks that drive fundamental biological processes such as pattern formation (Kondo and Asai, 1995; Meinhardt and Gierer, 2000; Sick et al., 2006) and development (Freeman, 2000; Materna and Davidson, 2007). The combination of these two functions allows each cell in a population to respond appropriately to local signals without the need for information regarding its position within the global system. Here, we have programmed a population of bacteria to form a pattern corresponding to the edges within a projected image of light. As in natural systems,

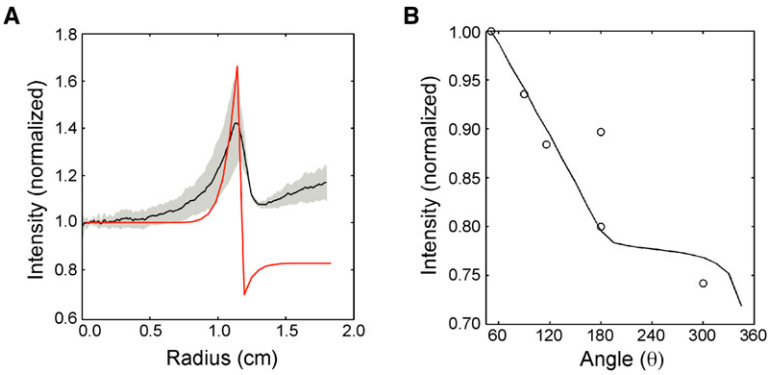

Figure 5. Quantitative Comparison of Model and Experimental Edges in One and Two Dimensions

(A) Comparison of the in vivo (black) and in silico (red) radial intensity profiles for the circle pattern. The average of three circle images (Figure S3) is shown along with the standard deviation (gray region) (Experimental Procedures).

(B) The relationship between the intersection angle (θ = degrees of light) of edges and the signal intensity is shown. Six points with five different θ values are sampled from the silhouette plate in Figure 4 (circles). The background intensity is subtracted from each point and the data is divided by the maximum intensity value. For each intersection angle, the maximum edge intensity is computed from the solution of the model with a unit circle mask with θ degrees of light (solid line) (Experimental Procedures).

communication greatly reduced the information-processing requirement for each member of the population while simple genetic logic allowed the proper integration of local signals for the formation of the final pattern.

Edge Detection is used for the identification of objects in a wide variety of *in silico* image processing applications (Suel et al., 2000) and has also been shown to be a natural function of the retina (Maturana and Frenk, 1963). *In silico* edge detection algorithms address each pixel of an image in series, resulting in a computation time that increases linearly with the number of pixels. In the bacterial edge detector the computation is massively parallel, resulting in a computation time that is independent of image size. This strategy is also an example of "Amorphous Computing" (Abelson et al., 2000) whereby a computation is performed as the emergent result of many spatially distributed processors working together locally without the need for global coordination. The applications of biological amorphous computers are still largely unexplored but are intriguing in light of the astounding feats of self-organization and information processing seen in natural pattern forming and neural network systems.

Several other efforts have leveraged cell-cell communication to program coordinated multicellular behaviors. These include a genetically-encoded turbidostat (You et al., 2004), one (Kobayashi et al., 2004) and two (Brenner et al., 2007) cell density-dependent transcription regulators, a transcriptional pulse generator (Basu et al., 2004), synthetic ecosystems (Balagadde et al., 2008; Weber et al., 2007) and a pattern forming system (Basu et al., 2005). In the latter case, two genetically distinct populations of bacteria (AHL senders and receivers) were manually overlayed in different configurations in order to generate different patterns. By contrast, the edge detector is implemented within an isogenic cell population that forms patterns in response to an external input with no requirements for cell placement.

Synthetic systems such as these could be used as early in vivo models for studying the 'design principles' that govern natural processes. Their simplicity and tractability makes them amenable to rigorous mathematical analysis, which can be used to generate rapidly testable hypotheses regarding the contribution of specific parameters to overall function. Because regulatory motifs recur ubiquitously in biology, the synthetic systems can then serve as working models for their natural counterparts (Sprinzak and Elowitz, 2005). The connection between primary DNA sequence and phenotype then closes the design cycle, expediting the engineering of novel biological behaviors.

The construction of very large fragments of DNA (Cello et al., 2002; Chan et al., 2005; Endy, 2008; Gibson et al., 2008a; Gibson et al., 2008b; Smith et al., 2003; Tumpey et al., 2005) is no longer a limitation in the engineering of biological systems. Predicting the behavior of complex genetic programs de novo is now the limiting step in the programming of cellular behavior. Thorough characterization of the performance of simple genetic parts and their resulting circuits will allow the development of predictive mathematical tools which will be required to program cells and cellular communities for functions which approach the sophistication of natural systems. This, in turn, will enable rigorous bottom-up testing of structure-function relationships in natural genetic systems.

EXPERIMENTAL PROCEDURES

Strain and Media

The strain for all experiments in this study is *E. coli* JW3367 (E. coli K12 W3110, *envZ-lacZ-* NCBI-GI: 89110606) from which the Kanamycin resistance marker is removed (termed JW3367c). Transformations are plated on LB agar supplemented with 50μg/mL Kanamycin, 34μg/mL Chloramphenicol and 50μg/mL Ampicillin as necessary. The strains are maintained in LB + 0.1M HEPES pH = 8.0 supplemented with the antibiotics. Glycerol stocks of the strains are maintained by adding 300 μL 60% glycerol (sterile) to 700μL actively growing culture (log phase) and freezing at −80°C.

Edge Detection Plasmids

E. coli JW3367c is transformed with the light sensing plasmids pPLPCB (p15a Kan^R) (Gambetta and Lagarias, 2001), pCph8 (ColE1, Cm^R) (Levskaya et al., 2005) and a third plasmid carrying the circuit. All of the circuit plasmids are based on the pSB4A3 BioBrick vector backbone (Shetty et al., 2008), which contains the pSC101* origin of replication and Amp^R. The pSC101* origin is carried at 2-3 copies per cell (Lutz and Bujard, 1997). The edge detector plasmid, pED_L3, is constructed from a series of DNA parts many of which are Biobricks (Knight, 2002) (see the Supplemental Data available with this article online). Other functional DNA elements used in the construction of the edge detector are the weak ribosome binding site RBS3(Weiss, 2001) and the ORF of the *lacZ* gene. The *lacZ* ORF is amplified from the plasmid pEXP*lacZ* (Invitrogen) using primers that encode the Biobricks prefix and suffix sequences, which carry the restriction sites EcoRI, XbaI (forward) and SpeI and PstI (reverse) respectively. This allows the *lacZ* gene to be cloned downstream of J13023 in its host plasmid via a suffix operation(Knight, 2002) using XbaI and PstI.

Photography, Inverter, and Communication Circuit Plasmids

The plasmids the carry the photography, inverter and cell-cell communication circuits are pJT108, pJT106 and pJT105, respectively. The plasmids pJT105 and pJT106 are constructed by deleting single genes from pED_L3 using seamless inverse PCR and ligation with the Phusion Site Directed Mutagenesis Kit (Finnzymes, Woburn, MA) according to manufacturer's instructions. Plasmid pJT108 is constructed by amplifying the $P_{ompC1157}$ genomic region of *E. coli* RU1012(Utsumi et al., 1989) with overhanging homology regions to pJT103 and seamlessly replacing R0082 via the MEGAWHOP method (Miyazaki, 2003). The $P_{ompC1157}$ promoter (pJT108) is used for the bacterial photographs because when read out by β-galactosidase directly, it produces smoother, higher contrast images than the shorter *ompC* promoter BBa_R0082.

Miller Assays

Miller Assays are conducted in 700 μL total volume with the Yeast β-Galactosidase Assay Kit (Pierce, Cat# 75768) in sterile, clear 1.7 mL microcentrifuge tubes at 28°C in ambient light according to the manufacturer's instructions. The reactions are quenched after visible yellow color develops and the OD_{420} measurements are taken in VWR disposable cuvettes (VWR Cat# 97000-586) on a Cary 50 Bio spectrophotometer. The equation to calculate Miller Units is $(1000*OD_{420})/(t*V*OD_{600})$, where t is the reaction time of the assay in minutes, and V is the volume of cell culture added to the reaction.

The Light Camera

A "Light Camera" (Incubator-Projector), which enables the projection of an image onto a plate of growing bacteria, is constructed as described before (Levskaya et al., 2005). A Kodak Ektagraphic III AMT projector equipped with an 82 V, 300 W Philips FocusLine quartz bulb is used as the light source. The broad wavelength light is filtered through a 650 nm bandpass filter (Edmund Optics catalog #43–189), stenciled through a 34x24 mm slide printed with a black and white image at 2032 dpi (mask), and focused through a lens. The images projected onto the slabs have power characteristics of 0.08 to 0.15 W/m^2 in the 620–680 nm band as determined by a EPP2000C Concave Grating spectrometer (Stellarnet, Oldsmar, FL). Dark areas of the images typically have 0.0000 to 0.0003 W/m^2 light over the same range. Bleedthrough light outside this band is negligible.

Plate-Based Assays

The output of the edge detector and other circuits are assayed using plates that are developed in the light camera. Detailed instructions for these assays are provided in the Supplemental Data. The agar slabs containing the bacteria are grown and exposed to light for 14 hr (Edge Detector, Inverter, Communication). The projector is then turned off and the slabs are allowed to 'develop' at 36°C in the dark for 10 hr. For photography the slabs are exposed to the image for 45 hr. The slabs are placed at 4°C overnight to stop bacterial growth and gene expression, before being photographed.

Image Analysis

Photographs of the bacterial plates are taken with a Canon SD900 digital camera. All four sample plates shown in Figure 3 of the main text were taken in a single photograph and the brightness, levels and contrasts were optimized identically. This preserves the relative signal intensity of each of the plates.

Determination of Background Intensity

The background intensity is measured to be 75 (where 0 is pure white and 255 is pure black), which is the "leaky" pixel intensity value taken from the illuminated region of the plate of bacteria expressing the inverter circuit in Figure 3C. This background intensity value is a constant through the entire image analysis.

Radial Edge Intensity Profiles

The radial edge intensity profiles in Figure 5A are extracted from the three circle images (Figure S3) (Matlab Image Processing Toolbox, Mathworks). These high resolution images are first converted to grayscale and subjected to a 5 point nearest neighbor smoothing to reduce digital artifacts. For each circle image, the radial pixel profile is calculated in the following way: starting from the center of each circle, the pixel intensities at each radial position (r = 0 to 2.8 cm) and at a constant θ coordinate are extracted. A set of radial pixel profiles are then extracted by performing this procedure while varying the θ coordinate. This set is then averaged together to create a mean radial pixel profile. This analysis is repeated for each circle image, creating a total of three independent mean radial pixel profiles. The background intensity is subtracted from each mean radial pixel profile. Then, each profile is divided by its radial pixel value at the r = 0 cm position, which is at the center of the circle, creating three independent fold-change edge profiles. The average and standard deviation of the fold-change edge profiles is computed.

Edge Intensity versus Angle

The raw grayscale pixel intensities from the asymmetrical silhouette mask are extracted at selected angle intersections (ImageJ, 1.40 g, Wayne Rasband, NIH) and background corrected. The background corrected intensities are then normalized by dividing by the maximum value in the data set (x = 51°, y = 1.0 in Figure 5B). The experimental values are compared to Miller Unit predictions from varying the angle of intersection in the reaction diffusion model as described below.

Determination of an Average Edge Width

The average edge width and error presented in the main text is determined by repeating three separate 36 mm circle pattern plates on three different days. The plates (Figure S3) are photographed and analyzed using ImageJ 1.40 g (Wayne Rasband, NIH). Raw images are converted to grayscale and inverted. The horizontal pixel intensity profile across the plate is determined using rectangle probe traversing the center of the circle. The width of the edge is determined from the pixel intensity profile by drawing a straight line from the start of the edge (point of rapid signal intensity rise) to the point at which the signal intensity drops to the approximate average maximum signal intensity in the nearby internal illuminated area. Two edges (one from the left side of the circle and one from the right) are measured on each plate. The individual widths measured from the three plates in Figure S3 are 0.86 cm, 0.76 cm, 0.46 cm, 0.62 cm, 0.37 cm, and 0.53 cm. The error values reported are the standard deviation.

Determination of the Dark Sensor Transfer Function, f_{light}

The transfer function of the dark sensor is determined in batch culture Miller Assay experiments using strain JW3367c carrying the plasmids pJT103, pPLPCB and pCph8. pJT103 is comprised of the shortened P_{ompC} promoter (BBa_R0082) upstream of the strong RBS (BBa_B0034) (Elowitz and Leibler, 2000) and the *lacZ* ORF in the pSB4A3 backbone (Figure S4).

Overnight starter cultures are inoculated from −80C stocks in 3 mL LB + Ampicillin, Kanamycin and Chloramphenicol and grown to OD_{600} ~4. Cultures are then diluted into 1 mL LB + 0.1M HEPES pH = 6.6 to a final OD_{600} of 0.001 and added to a single, internal well of a sterile 24-well plate (Falcon, Part# 351147). The plate (with lid on) is then fixed onto a VWR incubating mini shaker (Cat# 12620-942) from which the plastic lid has been removed, placed inside of a dark incubator, illuminated with a defined amount of 650 nm filtered light and shaken at 420 rpm for 330–345 min at 36°C. The light is measured as previously (Levskaya et al., 2005) with the spectrometer probe placed at the position equivalent to the *x,y* center of the assay plate. The cultures, which have reached log phase (final OD_{600} between 0.6 and 1.2), are immediately collected under a safe green light and pipetted into black 1.7 mL microcentrifuge tubes. Then, 100 μL of each sample is immediately used to determine the OD_{600} while 350 μL is used for the Miller Assay.

The quantity f_{light} is the expression rate of the light-repressed BioBrick *ompC* promoter as a function of light input and has been experimentally determined using a β-galactosidase readout (Figure 2A). We fit the experimental data to the sigmoidal function,

$$f_{light} = \frac{K}{K+L}(\beta_{max} - \beta_{min}) + \beta_{min} \quad (1)$$

where the fit parameter is K = 0.0017 W/m^2 (R^2 = 0.75), the maximum expression level β_{max} = 298 Miller Units, the minimum expression level β_{min} = 125 Miller Units, and the light intensity in units of W/m^2 passing through the mask at position (r, θ) is $L_{r,\theta}$.

Determination of the Logic Transfer Function, f_{logic}

The two-input transfer function of the signal integrating promoter $P_{lux-\lambda}$ (BBa_R0065) is determined in strain JW3367c carrying plasmids pJT104, pPLPCB and pCph8. pJT104 is the edge detection plasmid pED_L3 from which the *luxI* ORF (BBa_C0061) has been removed (Figure S5). This allows independent control of CI and AHL abundance via light and exogenous addition to the media, respectively. The readout of the $P_{lux-\lambda}$ (BBa_R0065) promoter is β-galactosidase in Miller Units.

The quorum signal $3OC_6HSL$ (N-(b-Ketocaproyl)-L-homoserine lactone, Sigma-Aldrich# K3007) is added at different concentrations across different wells of the plate while a single light intensity is applied to the entire plate. The data in Figure 2B are the result of 25 data points taken as 5 sets of 5 points over 5 days, where the 5 data points for a given light intensity are collected on a single day. The cell cultures are in mid-log phase and typically between OD_{600} 0.6 and 0.85 at the time of the assay.

The steady-state concentration of β-gal is determined by the transcription rate of the LuxR-activated, CI-repressed $P_{lux-\lambda}$ promoter, which is quantified by the f_{logic} function. The Shea-Ackers formalism is used to enumerate the binding states of LuxR and CI bound to the promoter (Ackers et al., 1982; Bintu et al., 2005b). The steady-state concentration of β-galactosidase is proportional to the probability of RNA polymerase initiating transcription. The expression for $f_{logic}(u_1,u_2)$ is

$$f_{logic}(u_1, u_2) = \frac{(c_0 + c_1 f_{Lux})}{1 + c_0 + c_1 f_{Lux} + c_2 f_{CI}^n + c_1 c_2 f_{Lux} f_{CI}^n} \quad (2)$$

where n = 1.5 and f_{Lux} is the concentration of LuxR dimer bound to AHL ($K_A^2 K_D^{LuxR}$ = 270,000 nM^3, $LuxR_{tot}$ = 2000 nM) (Urbanowski et al., 2004), which is

$$f_{Lux} = \frac{1}{2}\left[\left(LuxR_{tot} + \frac{K_A^2 K^{LuxR}}{4u_1^2}\right) - \sqrt{\left(LuxR_{tot} + \frac{K_A^2 K^{LuxR}}{4u_1^2}\right)^2 - LuxR_{tot}^2}\right] \quad (6)$$

and f_{CI} is the concentration of dimeric CI (K_D^{CI} = 5 nM (Koblan and Ackers, 1991)), which is

$$f_{CI} = \frac{u_2}{2} + \frac{1}{8K_D^{CI}}\left(1 - \sqrt{1 + 8K_D^{CI} u_2}\right) \quad (7)$$

The constants c_0 to c_2 reflect the apparent in vivo Gibbs free energies of binding for each state and are determined by minimizing the differences between the output of f_{logic} and the two-input transfer function over the 25 different conditions of $3OC_6HSL$ concentration and light intensity. The best fit values are $c_0 = 0.04$, $c_1 = 0.05$ and $c_2 = 0.011$ ($R^2 = 0.81$).

Reaction-Diffusion Model

Given a light mask, the reaction-diffusion model calculates the time- and position-dependent expression level of the β-galactosidase (β-gal) output gene. The model consists of (1) a partial differential equation describing $3OC_6HSL$ production, degradation, and diffusion and (2) two algebraic equations describing the steady-state concentrations of CI and β-gal in response to $3OC_6HSL$ and light. In dimensionless form, these equations are

$$\frac{\partial u_1}{\partial t^*} = \frac{1}{r^*}\frac{\partial u_1}{\partial r^*} + \frac{\partial^2 u_1}{\partial r^{*2}} + \frac{1}{r^{*2}}\frac{\partial^2 u_1}{\partial \theta^2} + \kappa_1 f_{light} - \kappa_2 u_1 \quad (8)$$

$$u_2 = \kappa_3 f_{light} \quad (9)$$

$$u_3 = \kappa_4 f_{logic}(u_1, u_2) \quad (10)$$

Where u_1, u_2, and u_3 represent the concentrations of $3OC_6HSL$, CI, and β-gal at a position on the plate whose polar coordinates are given by (r, θ). The f_{light} and f_{logic} functions quantify the transcription rates of the light-dependent *ompC* promoter and the CI-repressed, LuxR::$3OC_6HSL$-activated *lux-λ* promoter, respectively.

The constants κ_1 and κ_2 quantify the maximum production rate and the degradation rate of $3OC_6HSL$, respectively. The production rate of $3OC_6HSL$ is estimated so that the maximum concentration on the plate is 2.5 nM while the degradation rate of $3OC_6HSL$ is slow; it has a half-life of about 2.5 days at pH 6.6 (Flagan et al., 2003). The conversion factor between the *ompC* transcription rate, characterized by f_{light}, and CI concentration is $\kappa_3 = 0.8$ nM/Miller. The constant κ_4 is the maximum β-gal concentration, which is 289 Miller units. This value was determined in batch culture experiments as described above at 500 nM (maximum) exogenous AHL in the absence of any CI protein (plasmid pJT105).

When solving these equations, the space and time coordinates are dedimensionalized so that $r^* = r / R$ and $t^* = tD/R^2$ where r is the radial position from the center of the plate, R is the radius of the plate, t is time and D = 1.67×10^{-7} cm^2/sec is the diffusivity of $3OC_6HSL$ (Basu et al., 2005). The system is an agarose plate with radius R = 4.25 cm (3.55 mm operating depth), homogeneously filled with stationary bacteria. Because the bacterial photographs are crisp in our system we assume that there is no appreciable bacterial movement in the agarose plates. There is a no-flux boundary condition (Neumann type) at $r^* = 1$ and a uniformly zero initial $3OC_6HSL$ concentration.

The differential equations in Equations (8–10) are solved using the finite difference method. We substitute 2nd order central differences for all spatial derivatives to create a sparse system of ordinary differential equations. The ordinary differential equations are solved using the Matlab (Mathworks, Natick, MA) ode23 s stiff numerical integrator with a final time of 24 hr ($t^* = 0.0027$). A sufficient number of radial and axial elements are used to accurately resolve each light mask. The solution yields the dynamics of edge formation in response to a given light mask.

Quantifying the Effect of Angle of Intersection on Edge Intensity

The effect of changing the angle of intersection between light and dark boundaries on the edge intensity is examined, comparing the model predictions to the experimentally observed behaviors. We create a series of unit circle *in silico* masks where θ degrees of the circle are in the light with 360-θ degrees in the dark and where θ is varied from 50 to 345 degrees. For each mask, the solution of the reaction-diffusion model is computed, which predicts the maximum edge intensity. The maximum edge intensity is the β-galactosidase concentration at the edge location. The model predictions compare favorably with the experimentally observed edge intensities of the asymmetrical silhouette mask at the selected angle intersections (Figure 5B). The image analysis procedure to obtain the experimental data is described above.

Calculating the Radial β-gal Profile

The radial edge intensity profile of the circle images are compared to the in silico radial β-galactosidase profile from the model solution (Figure 5A). We compute the in silico radial β-galactosidase profile by first inputting the circle light mask into the model and determining the solution. Then, the β-galactosidase concentration in terms of Miller units (u_3) is outputted along the radial coordinate (r = 0 to 1.8 cm) and divided by the value of u_3 at r = 0 to obtain the normalized intensity in Figure 5A.

SUPPLEMENTAL DATA

Supplemental Data include Supplemental Experimental Procedures, five figures, and Supplemental References and can be found with this article online at http://www.cell.com/supplemental/S0092-8674(09)00509-1.

ACKNOWLEDGMENTS

We thank E.A. Davidson, L.A. Lavery, M. Levy, K. McGary, and A. Scouras for helpful discussions; A. Nishimura for the JW3367 *E. coli* strain; and L.A. Lavery, C. Conboy, and D. Endy for assistance with Biobrick construction. This work was supported by the National Science Foundation (SynBERC), NSF-BES0547637, NIH EY016546, NIH AI067699, NIH R01GM077040, Office of Naval Research, and the Pew and Packard Foundations. J.J.T. is supported by a Kirschstein National Research Service Award.

Received: January 30, 2009
Revised: March 9, 2009
Accepted: April 13, 2009
Published: June 25, 2009

REFERENCES

Abelson, H., Allen, D., Coore, D., Hanson, C., Homsy, G., Knight, T.F., Nagpal, R., Rauch, E., Sussman, G.J., Weiss, R., et al. (2000). Amorphous computing. Commun. ACM *43*, 74–82.

Ackers, G.K., Johnson, A.D., and Shea, M.A. (1982). Quantitative model for gene regulation by lambda phage repressor. Proc. Natl. Acad. Sci. USA *79*, 1129–1133.

Ajo-Franklin, C.M., Drubin, D.A., Eskin, J.A., Gee, E.P., Landgraf, D., Phillips, I., and Silver, P.A. (2007). Rational design of memory in eukaryotic cells. Genes Dev. *21*, 2271–2276.

Anderson, J.C., Clarke, E.J., Arkin, A.P., and Voigt, C.A. (2006). Environmentally controlled invasion of cancer cells by engineered bacteria. J. Mol. Biol. *355*, 619–627.

Anderson, J.C., Voigt, C.A., and Arkin, A.P. (2007). Environmental signal integration by a modular AND gate. Mol. Syst. Biol. *3*, 133.

Andrianantoandro, E., Basu, S., Karig, D.K., and Weiss, R. (2006). Synthetic biology: New engineering rules for an emerging discipline. Mol. Syst. Biol. *2*, 28.

Arkin, A.P., and Fletcher, D.A. (2006). Fast, cheap and somewhat in control. Genome Biol. *7*, 114.

Atkinson, M.R., Savageau, M.A., Myers, J.T., and Ninfa, A.J. (2003). Development of genetic circuitry exhibiting toggle switch or oscillatory behavior in Escherichia coli. Cell *113*, 597–607.

Balagadde, F.K., Song, H., Ozaki, J., Collins, C.H., Barnet, M., Arnold, F.H., Quake, S.R., and You, L. (2008). A synthetic Escherichia coli predator-prey ecosystem. Mol. Syst. Biol. *4*, 187.

Basu, S., Gerchman, Y., Collins, C.H., Arnold, F.H., and Weiss, R. (2005). A synthetic multicellular system for programmed pattern formation. Nature *434*, 1130–1134.

Basu, S., Mehreja, R., Thiberge, S., Chen, M.T., and Weiss, R. (2004). Spatiotemporal control of gene expression with pulse-generating networks. Proc. Natl. Acad. Sci. USA *101*, 6355–6360.

Benner, S.A., and Sismour, A.M. (2005). Synthetic biology. Nat. Rev. Genet. *6*, 533–543.

Bintu, L., Buchler, N.E., Garcia, H.G., Gerland, U., Hwa, T., Kondev, J., Kuhlman, T., and Phillips, R. (2005a). Transcriptional regulation by the numbers: applications. Curr. Opin. Genet. Dev. *15*, 125–135.

Bintu, L., Buchler, N.E., Garcia, H.G., Gerland, U., Hwa, T., Kondev, J., and Phillips, R. (2005b). Transcriptional regulation by the numbers: models. Curr. Opin. Genet. Dev. *15*, 116–124.

Brenner, K., Karig, D.K., Weiss, R., and Arnold, F.H. (2007). Engineered bidirectional communication mediates a consensus in a microbial biofilm consortium. Proc. Natl. Acad. Sci. USA *104*, 17300–17304.

Canton, B., Labno, A., and Endy, D. (2008). Refinement and standardization of synthetic biological parts and devices. Nat. Biotechnol. *26*, 787–793.

Cello, J., Paul, A.V., and Wimmer, E. (2002). Chemical synthesis of poliovirus cDNA: generation of infectious virus in the absence of natural template. Science *297*, 1016–1018.

Chan, L., Kosuri, S., and Endy, D. (2005). Refactoring bacteriophage T7. Mol. Syst. Biol *26*, 787.

Cox, R.S., 3rd, Surette, M.G., and Elowitz, M.B. (2007). Programming gene expression with combinatorial promoters. Mol. Syst. Biol *3*, 145.

Elowitz, M.B., and Leibler, S. (2000). A synthetic oscillatory network of transcriptional regulators. Nature *403*, 335–338.

Endy, D. (2005). Foundations for engineering biology. Nature *438*, 449–453.

Endy, D. (2008). Genomics. Reconstruction of the genomes. Science *319*, 1196–1197.

Engebrecht, J., and Silverman, M. (1984). Identification of genes and gene products necessary for bacterial bioluminescence. Proc. Natl. Acad. Sci. USA *81*, 4154–4158.

Flagan, S., Ching, W.K., and Leadbetter, J.R. (2003). Arthrobacter strain VAI-A utilizes acyl-homoserine lactone inactivation products and stimulates quorum signal biodegradation by Variovorax paradoxus. Appl. Environ. Microbiol. *69*, 909–916.

Freeman, M. (2000). Feedback control of intercellular signalling in development. Nature *408*, 313–319.

Fung, E., Wong, W.W., Suen, J.K., Bulter, T., Lee, S.G., and Liao, J.C. (2005). A synthetic gene-metabolic oscillator. Nature *435*, 118–122.

Gambetta, G.A., and Lagarias, J.C. (2001). Genetic engineering of phytochrome biosynthesis in bacteria. Proc. Natl. Acad. Sci. USA *98*, 10566–10571.

Gardner, T.S., Cantor, C.R., and Collins, J.J. (2000). Construction of a genetic toggle switch in Escherichia coli. Nature *403*, 339–342.

Gibson, D.G., Benders, G.A., Andrews-Pfannkoch, C., Denisova, E.A., Baden-Tillson, H., Zaveri, J., Stockwell, T.B., Brownley, A., Thomas, D.W., Algire, M.A., et al. (2008a). Complete chemical synthesis, assembly, and cloning of a Mycoplasma genitalium genome. Science *319*, 1215–1220.

Gibson, D.G., Benders, G.A., Axelrod, K.C., Zaveri, J., Algire, M.A., Moodie, M., Montague, M.G., Venter, J.C., Smith, H.O., and Hutchison, C.A., 3rd. (2008b). One-step assembly in yeast of 25 overlapping DNA fragments to form a complete synthetic Mycoplasma genitalium genome. Proc. Natl. Acad. Sci. USA *105*, 20404–20409.

Guet, C.C., Elowitz, M.B., Hsing, W., and Leibler, S. (2002). Combinatorial synthesis of genetic networks. Science *296*, 1466–1470.

Guido, N.J., Lee, P., Wang, X., Elston, T.C., and Collins, J.J. (2007). A pathway and genetic factors contributing to elevated gene expression noise in stationary phase. Biophys. J. *93*, 55–57.

Guido, N.J., Wang, X., Adalsteinsson, D., McMillen, D., Hasty, J., Cantor, C.R., Elston, T.C., and Collins, J.J. (2006). A bottom-up approach to gene regulation. Nature *439*, 856–860.

Ham, T.S., Lee, S.K., Keasling, J.D., and Arkin, A.P. (2006). A tightly regulated inducible expression system utilizing the fim inversion recombination switch. Biotechnol. Bioeng. *94*, 1–4.

Haseltine, E.L., and Arnold, F.H. (2007). Synthetic gene circuits: design with directed evolution. Annu. Rev. Biophys. Biomol. Struct. *36*, 1–19.

Kim, J.H., Kim, H.Y., and Lee, Y.S. (2001). A novel method using edge detection for signal extraction from cDNA microarray image analysis. Exp. Mol. Med. *33*, 83–88.

Kim, P.M., and Tidor, B. (2003). Limitations of quantitative gene regulation models: a case study. Genome Res. *13*, 2391–2395.

Knight, T. (2002). Idempotent vector design for the standard assembly of biobricks. MIT Synthetic Biology Working Group Technical Report 0.

Kobayashi, H., Kaern, M., Araki, M., Chung, K., Gardner, T.S., Cantor, C.R., and Collins, J.J. (2004). Programmable cells: interfacing natural and engineered gene networks. Proc. Natl. Acad. Sci. USA *101*, 8414–8419.

Koblan, K.S., and Ackers, G.K. (1991). Energetics of subunit dimerization in bacteriophage lambda cI repressor: linkage to protons, temperature, and KCl. Biochemistry *30*, 7817–7821.

Kondo, S., and Asai, R. (1995). A Reaction-Diffusion Wave on the Skin of the Marine Angelfish Pomacanthus. Nature *376*, 765–768.

Kramer, B.P., and Fussenegger, M. (2005). Hysteresis in a synthetic mammalian gene network. Proc. Natl. Acad. Sci. USA *102*, 9517–9522.

Kramer, B.P., Viretta, A.U., Daoud-El-Baba, M., Aubel, D., Weber, W., and Fussenegger, M. (2004). An engineered epigenetic transgene switch in mammalian cells. Nat. Biotechnol. *22*, 867–870.

Levskaya, A., Chevalier, A.A., Tabor, J.J., Simpson, Z.B., Lavery, L.A., Levy, M., Davidson, E.A., Scouras, A., Ellington, A.D., Marcotte, E.M., et al. (2005). Synthetic biology: engineering Escherichia coli to see light. Nature *438*, 441–442.

Lutz, R., and Bujard, H. (1997). Independent and tight regulation of transcriptional units in Escherichia coli via the LacR/O, the TetR/O and AraC/I1–I2 regulatory elements. Nucleic Acids Res. *25*, 1203–1210.

Materna, S.C., and Davidson, E.H. (2007). Logic of gene regulatory networks. Curr. Opin. Biotechnol. *18*, 351–354.

Maturana, H.R., and Frenk, S. (1963). Directional Movement and Horizontal Edge Detectors in the Pigeon Retina. Science *142*, 977–979.

Mayo, A.E., Setty, Y., Shavit, S., Zaslaver, A., and Alon, U. (2006). Plasticity of the cis-regulatory input function of a gene. PLoS Biol. *4*, e45. 10.1371/journal.pbio.0040045.

Meinhardt, H., and Gierer, A. (2000). Pattern formation by local self-activation and lateral inhibition. Bioessays *22*, 753–760.

Miyazaki, K. (2003). Creating random mutagenesis libraries by megaprimer PCR of whole plasmid (MEGAWHOP). Methods Mol. Biol. *231*, 23–28.

Purnick, P.E., and Weiss, R. (2009). The second wave of synthetic biology: from modules to systems. Nat. Rev. Mol. Cell. Biol. *10*, 410–422.

Rackham, O., and Chin, J.W. (2005). Cellular logic with orthogonal ribosomes. J. Am. Chem. Soc. *127*, 17584–17585.

Shea, M.A., and Ackers, G.K. (1985). The OR control system of bacteriophage lambda. A physical-chemical model for gene regulation. J. Mol. Biol. *181*, 211–230.

Shetty, R.P., Endy, D., and Knight, T.F., Jr. (2008). Engineering BioBrick vectors from BioBrick parts. J. Biol. Eng. *2*, 5.

Sick, S., Reinker, S., Timmer, J., and Schlake, T. (2006). WNT and DKK determine hair follicle spacing through a reaction-diffusion mechanism. Science *314*, 1447–1450.

Smith, H.O., Hutchison, C.A., 3rd, Pfannkoch, C., and Venter, J.C. (2003). Generating a synthetic genome by whole genome assembly: phiX174 bacteriophage from synthetic oligonucleotides. Proc. Natl. Acad. Sci. USA *100*, 15440–15445.

Sprinzak, D., and Elowitz, M.B. (2005). Reconstruction of genetic circuits. Nature *438*, 443–448.

Stricker, J., Cookson, S., Bennett, M.R., Mather, W.H., Tsimring, L.S., and Hasty, J. (2008). A fast, robust and tunable synthetic gene oscillator. Nature *456*, 516–519.

Suel, M., O'Gorman, L., and Sammon, M.J. (2000). Practical Algorithms for Image Analysis.

Tabor, J.J., Bayer, T.S., Simpson, Z.B., Levy, M., and Ellington, A.D. (2008). Engineering stochasticity in gene expression. Mol. Biosyst. *4*, 754–761.

Tabor, J.J., Groban, E.S., and Voigt, C.A. (2009). Performance characteristics for sensors and circuits used to program E.coli. In Systems Biology and Biotechnology of Escherichia coli, S.Y. Lee, ed. (New York: Springer), pp. 401–439.

Tigges, M., Marquez-Lago, T.T., Stelling, J., and Fussenegger, M. (2009). A tunable synthetic mammalian oscillator. Nature *457*, 309–312.

Tumpey, T.M., Basler, C.F., Aguilar, P.V., Zeng, H., Solorzano, A., Swayne, D.E., Cox, N.J., Katz, J.M., Taubenberger, J.K., Palese, P., et al. (2005). Characterization of the reconstructed 1918 Spanish influenza pandemic virus. Science *310*, 77–80.

Urbanowski, M.L., Lostroh, C.P., and Greenberg, E.P. (2004). Reversible acyl-homoserine lactone binding to purified Vibrio fischeri LuxR protein. J. Bacteriol. *186*, 631–637.

Utsumi, R., Brissette, R.E., Rampersaud, A., Forst, S.A., Oosawa, K., and Inouye, M. (1989). Activation of bacterial porin gene expression by a chimeric signal transducer in response to aspartate. Science *245*, 1246–1249.

Voigt, C.A. (2006). Genetic parts to program bacteria. Curr. Opin. Biotechnol. *17*, 548–557.

Weber, W., Daoud-El Baba, M., and Fussenegger, M. (2007). Synthetic ecosystems based on airborne inter- and intrakingdom communication. Proc. Natl. Acad. Sci. USA *104*, 10435–10440.

Weiss, R. (2001). Cellular Computation and Communications Using Engineered Genetic Regulatory Networks.

Weiss, R., Homsy, G.E., and Knight, T.F., Jr. (1999). Toward in vivo digital circuits. DIMACS Workshop on Evolution as Computation *1*, 1–18.

Weiss, R., and Knight, T.F., Jr. (2001). Engineering Communications for Microbial Robotics. In Lecture Notes In Computer Science (Heidelberg: Springer), pp. 1–16.

Yeh, K.C., Wu, S.H., Murphy, J.T., and Lagarias, J.C. (1997). A cyanobacterial phytochrome two-component light sensory system. Science *277*, 1505–1508.

Yokobayashi, Y., Weiss, R., and Arnold, F.H. (2002). Directed evolution of a genetic circuit. Proc. Natl. Acad. Sci. USA *99*, 16587–16591.

You, L., Cox, R.S., 3rd, Weiss, R., and Arnold, F.H. (2004). Programmed population control by cell-cell communication and regulated killing. Nature *428*, 868–871.